

Efficient Polynomial-Scaled Determination of Algebraic Entanglement Entropy Between Collective Degrees of Freedom

John Drew Wilson^{1,2,*}, Jarrod T. Reilly^{1,2,*}, and Murray J. Holland^{1,2}

¹JILA, ²NIST, and ³Department of Physics, University of Colorado, 440 UCB, Boulder, CO 80309, USA

In this work, we explore physical systems which support not only multipartite *interparticle* entanglement, but also *intraparticle* entanglement between different degrees of freedom of the constituent particles and entanglement between different degrees of freedom of different particles, i.e., *algebraic* entanglement. We derive a simple method for calculating the algebraic entanglement entropy between two of the particles' degrees of freedom from collective states of the whole ensemble. Our procedure makes use of underlying symmetries in these systems, in particular permutation symmetry of the particle indices, and shows a connection between the algebraic entanglement entropy in these systems and the irreducible representations of Lie groups which describe the particles' degrees of freedom. Namely, we use the direct sum over irreducible representations to diagonalize the reduced density matrices in a block-by-block manner, then utilize the multiplicity of these irreducible representations to reproduce the results from an exponentially-scaled Hilbert space in only polynomial complexity. We use this to explore a variety of systems where the constituent particles support two degrees of freedom each with two levels, such as atoms with two electronic states and two momentum states. Notably, these systems may be exactly simulated in a polynomial-scaled Hilbert space, yet they support an algebraic entanglement entropy that grows linearly with the particle number which typically requires an exponentially-scaled Hilbert space.

I. INTRODUCTION

Quantum entanglement is one of the most striking features of quantum mechanics with no classical analog. This makes technologies that utilize quantum entanglement promising for use in improved sensing [1–7], computing [8–12], simulation [13–17], and more [18–26]. Entanglement is crucial to these technologies because non-local correlations between subsystems can be exploited to surpass the capabilities of classical devices, such as overcoming the standard quantum limit [1, 3, 4] or teleporting information from a source to destination [27–29]. Due to its importance, many theoretical techniques have been developed to detect, characterize, and analyze the entanglement in a quantum system, e.g., quantum Fisher information [1, 30, 31], quantum state tomography [32–34], and the Schmidt decomposition [18, 35, 36].

Of primary interest in this work is the concept of entanglement entropy [18, 36, 37] which characterizes the degree of entanglement between two subsystems of a quantum device and is of fundamental interest to quantum theory [37–39]. The most simple quantum system which supports entanglement is a bipartite system, where the whole may be divided into two composite systems. Here, calculating the entanglement entropy is relatively straightforward because it only involves tracing out one subsystem before subsequently diagonalizing the resultant density matrix to calculate its entropy. As a result, bipartite systems, have long been the workhorses in quantum information processing [40] and fundamental tests of quantum theory [41, 42]. The natural extension of bipartite systems are multipartite systems, in which multiple subsystems must be traced out before diagonalizing the resultant density matrix [43], and which are central to many interesting tasks in quantum information [44, 45].

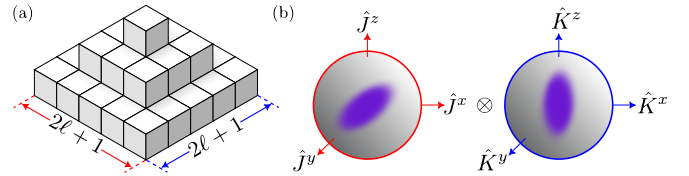


FIG. 1. (a) A cartoon of the pyramid structure of the $SU(4)$ state space. Each layer of the pyramid is a square of size $(2\ell + 1)$ -by- $(2\ell + 1)$ for the $(2\ell + 1)$ -many levels of each degree of freedom. (b) The two Bloch spheres with dipole length ℓ for the $SU(2) \otimes SU(2)$ subgroup of $SU(4)$. Layer ℓ of the state space in (a) corresponds to many copies of this subgroup.

Recently, there has been growing interest in physical processes that generate not only multipartite *interparticle* entanglement, but also *intraparticle* entanglement amongst multiple degrees of freedom of a single particle or, more generally, entanglement between different degrees of freedom of different particles. Borrowing terminology from quantum field theory, we will refer to entanglement between different degrees of freedom of many-body states as *algebraic* entanglement [46–48] between degrees of freedom to distinguish it from multipartite entanglement between atoms irregardless of the degrees of freedom. A special case of this kind of entanglement is hybrid entanglement between a discrete degree of freedom and a continuous degree of freedom [49–56], but we can also use algebraic entanglement to encapsulate entanglement between two discrete (or two continuous) degrees of freedom in collective many-body states. These systems typically involve the internal energy levels of an atom as well as the external spatial degrees of freedom [1, 57–67] where the entanglement can be relevant for processes such as multi-parameter sensing [1], thermalization [68], and entropy removal via laser cooling [69–72]. Therefore, one would like to calculate the algebraic entanglement entropy between two or more degrees of freedom across the whole of the particle ensemble. However, the process of unraveling these degrees of freedom by tracing

* These authors contributed equally to this work. Corresponding author: Jarrod.Reilly@colorado.edu

one out is generally computationally expensive. For example, naively using the single-particle basis to trace out one degree of freedom scales exponentially with the number of particles which makes it intractable other than for a few particles.

In this paper, we describe how to utilize symmetries of a system and representation theory to calculate information theoretic quantities efficiently in polynomial complexity. We present a deep connection between the algebraic entanglement entropy amongst collections of particles with multiple degrees of freedom and the structure of Lie groups which describe these degrees of freedom. We focus on the simplest case of an ensemble whose constituent particles have two degrees of freedom, such as spin and momentum, and both degrees of freedom only have two states. In this case, we make use of the subgroup structure of $SU(4)$ to trace out one of the degrees of freedom by finding an efficient direct mapping into a representative class of reduced density matrices which preserves the polynomial-scaling of the bosonic subspace of $SU(4)$. After tracing out one degree of freedom, we are left with a direct sum over density matrices describing the other degree of freedom using the irreducible representations (irreps) of $SU(2)$. As a consequence, the reduced density matrix in one of the subsystems takes on a block diagonal form which is again polynomial-scaled [73]. We also provide a natural depiction of the state space into a pyramid structure, where each layer of the pyramid provides a representation of $SU(2) \otimes SU(2)$, i.e., two “spin-ladders” of equal lengths, as depicted in the cartoon of Fig. 1.

Systems with this structure naturally appear in experiments where atoms are collectively coupled through a resonator, such as an optical cavity [15, 57, 67, 74, 75]. The use of the $SU(4)$ group structure allows one to reduce the scaling of computations from exponential 4^N , to polynomial $\mathcal{O}(N^3)$, where N is the number of constituent particles. This allows theoretical studies to perform exact simulations for $N \gg 1$ while keeping track of all interparticle and intraparticle correlations. Moreover, the pyramid structure presented here and in Ref. [73] greatly reduces the task of both taking the trace and diagonalizing the density matrix in order to calculate quantities such as the quantum Fisher information [31] and entanglement entropy [18]. This is because these procedures can be performed in a block-by-block manner, the largest of which only scales as $\mathcal{O}(N^2)$, which is a massive reduction of numerical complexity compared to the single-particle basis.

While we focus on the case $SU(2) \otimes SU(2) < SU(4)$ here, where $<$ denotes a subgroup, our methodology can be extended to systems where each degree of freedom of the constituent particles possess a Lie group structure which can be decomposed into its irreps. Counterintuitively, we show that the entanglement entropy S_E in these systems grows linearly with the number of constituent particles, $S_E = \mathcal{O}(N)$, rather than with the logarithm of the dimension of the polynomial-scaled Hilbert space, $S_E = \mathcal{O}(\ln(N))$, which is only possible due to the multiplicity (number of copies) of the irreps. This is a signature of complex particle-particle correlated physics that is a result of collective interactions in non-bosonic representations of the different degrees of freedom. All of this leads to interesting, highly entangled physics which is straightforward

to simulate in polynomial complexity with respect to N .

The paper is structured as follows. We begin in Sec. II with an illustrative example of the $SU(4)$ systems we consider in order to highlight the computational complexity of calculating algebraic entanglement entropy in the single-particle basis. We then turn to the symmetry properties and representation theory that allows us to reduce the computational complexity to polynomial-scaling in Sec. III. In Sec. IV, we present the full algorithm to calculate algebraic entanglement entropy by mapping the bosonic subspace of $SU(4)$ to the irreps of $SU(2)$. In Sec. V, we provide a number of physical examples of both closed and open quantum systems where we apply our algebraic entanglement entropy algorithm. We finish with some concluding remarks in Sec. VI.

II. ILLUSTRATIVE EXAMPLE

Before diving into the mathematical structure that we exploit to perform polynomial-scaled calculations of algebraic entanglement entropy, we first consider a simple physical example that can be solved analytically. In this example, we can calculate the entanglement entropy by straightforward physical arguments. However, we highlight that with more complicated $SU(4)$ dynamics, direct methods are extremely computationally demanding without exploiting permutation symmetry and representation theory.

Consider a pulse from counterpropagating lasers applied to a cloud of N atoms, driving a transition between two internal levels of the atoms, labeled $|0\rangle$ and $|1\rangle$ for ground and excited state, respectively. We assume that the atoms only have momentum along the lasers’ axes, which we label the z -direction. By conservation of momentum, the atoms will experience a corresponding momentum impulse of $\pm\hbar k$ when absorbing or emitting photons from the lasers, where k is the wavenumber of the photons. During the time t the pulse is applied for, the Hamiltonian of the system is given by

$$\hat{H}_{\text{CPL}} = \sum_{j=1}^N \frac{\hat{p}_j^2}{2m} + \frac{\hbar\Delta}{2} \hat{\sigma}_j^z + \hbar\Omega \cos(k\hat{z}_j) \hat{\sigma}_j^x, \quad (1)$$

where \hat{z}_j is the position operator of atom j , \hat{p}_j is the momentum operator, and $\hat{\sigma}_\mu^{(j)}$ is a Pauli operator with $\mu \in \{x, y, z\}$. Here, we have assumed that the lasers have the same Rabi frequency Ω and a fixed detuning Δ from the atomic transition frequency. When the energy of the photons is insufficient to drive the atoms to higher momentum states, as is the case in Refs. [1, 57, 67], one is able to truncate the atomic motion to just two momentum states, $|\uparrow\rangle_j \equiv |+\hbar k/2\rangle_j$ and $|\downarrow\rangle_j \equiv |-\hbar k/2\rangle_j$, assuming the atoms began with its population completely in these states. In principle, there could be a momentum offset such as $|p_0 \pm \hbar k/2\rangle$ or the two momentum states could be separated by a multiple of $\hbar k$ and driven by multi-photon processes [7], but we will only consider $|\uparrow\rangle_j$ and $|\downarrow\rangle_j$ here. We can then trace out the remainder of the

momentum basis such that the Hamiltonian becomes

$$\hat{H}_{\text{IE}} = \sum_{j=1}^N \frac{\hbar\Delta}{2} \hat{\sigma}_j^z + \frac{\hbar\Omega}{2} \hat{\sigma}_j^x \otimes \hat{s}_j^x, \quad (2)$$

where we have dropped a constant kinetic energy shift of $N\hbar^2k^2/(8m)$.

We can now study how the algebraic entanglement between the internal states and momentum states grows throughout the pulse duration. To do so, we assume the atoms are initially in the ground state with a momentum of $-\hbar k/2$: $|\Psi(0)\rangle = \bigotimes_{j=1}^N (|0\rangle_j \otimes |\downarrow\rangle_j)$. Since Eq. (2) has no particle-particle interactions, we know the final state is separable atom-by-atom, i.e., $|\Psi(t)\rangle = \bigotimes_{j=1}^N |\psi(t)\rangle_j$. This observation will allow us to calculate the algebraic entanglement entropy simply. The state of atom j may be solved for [76]

$$\begin{aligned} |\psi(t)\rangle_j = & e^{-\frac{i\Delta t}{2}} \left[\cos\left(\frac{\tilde{\Omega}t}{2}\right) + \frac{i\Delta}{\tilde{\Omega}} \sin\left(\frac{\tilde{\Omega}t}{2}\right) \right] |0\rangle_j \otimes |\downarrow\rangle_j \\ & - i e^{-\frac{i\Delta t}{2}} \frac{\Omega}{\tilde{\Omega}} \sin\left(\frac{\tilde{\Omega}t}{2}\right) |1\rangle_j \otimes |\uparrow\rangle_j, \end{aligned} \quad (3)$$

where $\tilde{\Omega} = \sqrt{\Omega^2 + \Delta^2}$ is the generalized Rabi frequency. In the case that the drive is on resonance with the transition frequency, $\Delta = 0$, then at time $t_{\text{max}} = \pi/(2\Omega)$ we find the state

$$|\Psi_{\text{max}}\rangle = \bigotimes_{j=1}^N \frac{1}{\sqrt{2}} (|0\rangle_j \otimes |\uparrow\rangle_j - i |1\rangle_j \otimes |\downarrow\rangle_j), \quad (4)$$

which, notably, has maximum algebraic entanglement between atom j 's internal and momentum states. We can see this by first tracing out either the internal states or the momentum states. For notational clarity, we identify the two degrees of freedom by the labels J and K for the internal and external degrees of freedom, respectively. The reduced density matrices are then $\hat{\rho}_J(t) = \text{Tr}_K[\hat{\rho}(t)]$ and $\hat{\rho}_K(t) = \text{Tr}_J[\hat{\rho}(t)]$ for the density matrix $\hat{\rho}(t) = |\Psi(t)\rangle\langle\Psi(t)|$, where Tr_i denotes the partial trace over subsystem i . We can then calculate the entanglement entropy by finding the von Neumann entropy of the reduced density matrices,

$$S_E[\hat{\rho}_J(t)] = -\text{Tr}[\hat{\rho}_J(t) \ln \hat{\rho}_J(t)] = S_E[\hat{\rho}_K(t)]. \quad (5)$$

The second equality holds for pure states by the monogamy of entanglement [18]. It is straightforward to show that the state given by Eq. (4) will have entanglement entropy scaling as

$$S_E[\hat{\rho}_{J,\text{max}}] = N \ln 2, \quad (6)$$

after noting that the reduced density matrix becomes the normalized 2^N -dimensional identity operators after taking the partial trace,

$$\hat{\rho}_{J,\text{max}} = \text{Tr}_K(|\psi_{\text{max}}\rangle\langle\psi_{\text{max}}|) = \frac{1}{2^N} \hat{\mathbb{I}}_{2^N}. \quad (7)$$

Notably, this yields an algebraic entanglement entropy that scales linearly with N , rather than the natural log of N . This

linear scaling of the entanglement entropy is typically indicative of a Hilbert space which grows exponentially.

Note that the state Eq. (4) has maximal algebraic entanglement while having no particle-particle entanglement. This means that the state would be extremely useful for quantum information science such as quantum teleportation between the two degrees of freedom, but would provide no quantum advantage beyond the standard quantum limit in quantum metrology. In this case, the algebraic entanglement entropy is thus purely intraparticle entanglement between the degrees of freedom of each atom. However, in more general systems, the calculation in Eq. (5) cannot differentiate this intraparticle entanglement from entanglement between, e.g., the J degree of freedom of atom i and the K degree of freedom of atom j ($i \neq j$). Moreover, the state with maximal hyperentanglement [77, 78], $|\Psi_{\text{HE,max}}\rangle = |\Phi\rangle_J \otimes |\Xi\rangle_K$ where $|\Phi\rangle_J$ and $|\Xi\rangle_K$ are symmetric N -particle Greenberger–Horne–Zeilinger (GHZ) states on the respective degree of freedom, has no algebraic entanglement between J and K under Eq. (5). This is why we distinguish the algebraic entanglement calculated in Eq. (5) from intraparticle entanglement, multipartite entanglement between atoms, and hyperentanglement, while hybrid entanglement is a special case of algebraic entanglement with J being discrete and K being continuous or vice versa. Here, ‘‘algebraic’’ refers to the algebras associated with the symmetries of the respective degrees of freedom. In the case above, we are calculating the entanglement between the $\mathfrak{su}(2)$ Lie algebra associated with J and the $\mathfrak{su}(2)$ Lie algebra associated with K , as discussed further in the next section.

In systems where the Hamiltonian (or jump operators) contain interparticle interactions, the exponential scaling of the Hilbert space would typically make the above analytical calculation of the algebraic entanglement entropy infeasible. This is the case when considering the systems presented in, e.g., Refs. [57, 67] in which the dynamics are solved using a second quantization formalism which abstracts away the single-particle dynamics. On first pass, it appears that this makes calculating the algebraic entanglement entropy both analytically and numerically impossible for $N \gg 1$ because of the exponential-scaling of the single-particle basis. Decomposing the state into single-particle dynamics is not possible, and therefore tracing out one of these degrees of freedom appears to require knowledge about individual particle-particle correlations, while diagonalizing the density matrix necessitates addressing the whole Hilbert space. As a result, general calculations of S_E are far more difficult.

In the following section, we will outline the state space needed to compute general dynamics of this form in order to show that the space of bosonic wavefunctions naturally admits an algebraic decomposition following from the structure of $\text{SU}(2) \otimes \text{SU}(2) < \text{SU}(4)$. This, we will show, allows the algebraic entanglement entropy to be calculated efficiently using representation theory in all cases that the constituent particles possess permutational symmetry.

III. BOSONIC SUBSPACE OF SU(4)

We now turn to the general group structure that we focus on throughout this paper. As in the previous example, we consider permutationally symmetric particles with two intra-particle degrees of freedom. We also assume the constituent degrees of freedom of each particle are themselves two-level systems, such that they admit a $SU(2) \otimes SU(2) < SU(4)$ structure. This could therefore relate to atoms with a two-level electronic manifold and two momentum states [1, 57, 67] or two relevant hyperfine states [15], molecules with two electronic and two vibrational states, two distinguishable spinor Bose-Einstein condensates in an optical lattice, or even an atom with two correlated spatial degrees of freedom. We now give an brief overview of algebraic operators that generate the system's dynamics in these systems, describe how they connect to the Lie group SU(4) for permutation symmetric systems, and then introduce a state space that allows for the polynomial-scaled entanglement entropy algorithm presented in Sec. IV.

A. SU(4) Operators

The operator space we consider is given by

$$\hat{G}_{\mu\nu} \equiv \sum_{j=1}^N \hat{\sigma}_{\mu}^{(j)} \otimes \hat{s}_{\nu}^{(j)}, \quad (8)$$

for $\mu, \nu \in \{I, x, y, z, (+), (-)\}$ and Pauli matrices $\hat{\sigma}_{\mu}^{(j)}$ and $\hat{s}_{\nu}^{(j)}$ acting on the first or second degree of freedom of particle j . The operators are shown explicitly in Appendix A. Additionally, $\hat{\sigma}_I^{(j)} = \hat{s}_I^{(j)} = \hat{\mathbb{1}}_2$ is the two-by-two identity operator on each space so that \hat{G}_{II} is the identity operator on the whole system's vector space. Considering just the Hermitian operators $\mu, \nu \in \{I, x, y, z\}$, one can build a 15-dimensional operator basis for the $\mathfrak{su}(4)$ Lie algebra [1] which, under exponentiation, generates SU(4). These are simply linear combinations of the traditional Gell-Mann matrices [79]. The two distinguishable degrees of freedom we care about will again be labeled J and K , and correspond to the $\mathfrak{su}(2)$ sub-algebras given by the operators $\hat{J}_{\mu} \equiv \hat{G}_{\mu I}/2$ and $\hat{K}_{\nu} \equiv \hat{G}_{I\nu}/2$, which are sums over all particles of the Pauli matrices $\mu, \nu \in \{x, y, z\}$ on only one degree of freedom. For the raising/lowering operators $\mu, \nu \in \{(+), (-)\}$, we have the collective ladder operators $\hat{J}_{\pm} \equiv \hat{G}_{(\pm)I}$ and $\hat{K}_{\pm} \equiv \hat{G}_{I(\pm)}$. Meanwhile, operators that are not in the respective $\mathfrak{su}(2)$ sub-algebras, $\hat{G}_{(\mu \neq I)(\nu \neq I)}$, represent SU(4) operators that generate algebraic entanglement between the J and K degrees of freedom (sub-algebras).

B. State Space

The key to efficiently calculating the algebraic entanglement entropy in general is the symmetry underlying the state space. In particular, we assume that the atoms remain in a

permutationally symmetric subspace, i.e. the state remains symmetric under the exchange of particle indices, whereupon calculating the reduced density matrices is greatly simplified. This vector space is a basis of the bosonic irrep of the group SU(4) and, as we will see, contains many copies of the SU(2) subgroups for J and K . The total single-particle state space, labeled \mathcal{H}_{tot} , scales exponentially as $\dim(\mathcal{H}_{\text{tot}}) = 4^N$. The use of permutation symmetry, however, reduces the size of the state space from exponential size to polynomial, $\dim(\mathcal{H}_{\text{sym}}) = (N+1)(N+2)(N+3)/6 \sim N^3$ [73]. Here, \mathcal{H}_{sym} is the space of states of the form

$$|\alpha, \beta, \gamma, \delta\rangle = \mathcal{S} \left(|1, \uparrow\rangle^{\otimes \alpha} |1, \downarrow\rangle^{\otimes \beta} |0, \uparrow\rangle^{\otimes \gamma} |0, \downarrow\rangle^{\otimes \delta} \right), \quad (9)$$

where \mathcal{S} is the symmetrizer and normalization dictates that $\alpha + \beta + \delta + \gamma = N$. The method of Schwinger bosons [80] is often used to describe dynamics on this space, whereupon each state is described as a mode with particles created and annihilated therein. This allows one to solve the dynamics in a general second quantization picture, but yields no insight into the algebraic entanglement entropy between J and K . An equivalent and far more convenient basis can be found through the following observation.

Consider the case of two particles, $N = 2$. The state

$$\frac{1}{2} (|0\rangle_1 |1\rangle_2 - |1\rangle_1 |0\rangle_2) \otimes (|\uparrow\rangle_1 |\downarrow\rangle_2 - |\downarrow\rangle_1 |\uparrow\rangle_2) \quad (10)$$

is permutationally symmetric because permuting the particles permutes the label in both the spin and momentum basis. In other words, the total state remains symmetric if both degrees of freedom are in an anti-symmetric singlet pair. On the other hand, if one degree of freedom is in one of the symmetric triplet states,

$$\begin{aligned} &|0\rangle_1 |0\rangle_2, \quad |1\rangle_1 |1\rangle_2, \quad \frac{1}{\sqrt{2}} (|0\rangle_1 |1\rangle_2 + |1\rangle_1 |0\rangle_2), \\ &|\downarrow\rangle_1 |\downarrow\rangle_2, \quad |\uparrow\rangle_1 |\uparrow\rangle_2, \quad \frac{1}{\sqrt{2}} (|\downarrow\rangle_1 |\uparrow\rangle_2 + |\uparrow\rangle_1 |\downarrow\rangle_2), \end{aligned} \quad (11)$$

then the other degree of freedom must also be in one of the triplet states for the total state to be in the symmetric SU(4) subspace of the two particles. Using the Young tableaux technique to find the irreps of the permutation group S_n and SU(n) [79, 81, 82], this argument can be extended to the full ensemble of particles so that both degrees of freedom must have the same number of singlet pairs, i.e., be in the same irrep of the SU(2) subgroups, for the total state to be in the symmetric SU(4) subspace [73]. In simpler terms, the anti-symmetry of particle exchange in each degree of freedom has to be exactly the same in order to result in a net symmetry under particle exchange.

The states in Eqs. (10) and (11) could equivalently be labeled by the eigenvalues of the collective z -operators and Casimir

operators of the SU(2) subgroups,

$$\begin{aligned} \hat{J}_z &= \frac{\hat{G}_{zI}}{2}, & \hat{J}^2 &= \sum_{\mu=x,y,z} (\hat{J}_\mu)^2 = \sum_{\mu=x,y,z} \left(\frac{\hat{G}_{\mu I}}{2} \right)^2, \\ \hat{K}_z &= \frac{\hat{G}_{Iz}}{2}, & \hat{K}^2 &= \sum_{\nu=x,y,z} (\hat{K}_\nu)^2 = \sum_{\nu=x,y,z} \left(\frac{\hat{G}_{I\nu}}{2} \right)^2. \end{aligned} \quad (12)$$

The Dicke states $|j, m_j\rangle$ and $|k, m_k\rangle$ are then eigenvectors of these operators with eigenvalues given by $\hat{J}_z |j, m_j\rangle = m_j |j, m_j\rangle$, $\hat{J}^2 |j, m_j\rangle = j(j+1) |j, m_j\rangle$, $\hat{K}_z |k, m_k\rangle = m_k |k, m_k\rangle$, and $\hat{K}^2 |k, m_k\rangle = k(k+1) |k, m_k\rangle$. The two-particle triplet states are then

$$\begin{aligned} &|j=1, m_j=1\rangle, & |j=1, m_j=0\rangle, & |j=1, m_j=-1\rangle, \\ &|k=1, m_k=1\rangle, & |k=1, m_k=0\rangle, & |k=1, m_k=-1\rangle, \end{aligned} \quad (13)$$

while the singlet states are

$$|j=0, m_j=0\rangle, \quad |k=0, m_k=0\rangle. \quad (14)$$

This leads to the important observation that, so long as both degrees of freedom have the same Casimir eigenvalue $j = k$, the overall wavefunction will remain permutationally symmetric. Extending this to the total ensemble of particles [83], we can thus label an orthonormal basis of the total bosonic representation of SU(4) as $|\ell, m_j, m_k\rangle$, where

$$\hat{J}^2 |\ell, m_j, m_k\rangle = \hat{K}^2 |\ell, m_j, m_k\rangle = \ell(\ell+1) |\ell, m_j, m_k\rangle. \quad (15)$$

This new basis is equivalent to the $|\alpha, \beta, \gamma, \delta\rangle$ basis, where we technically only need to specify three quantum numbers α, β, γ to fully specify a state because $\delta = N - \alpha - \beta - \gamma$. The two bases uniquely map into each other through $m_j = (\alpha + \beta - \gamma - \delta)/2$, and $m_k = (\alpha - \beta + \gamma - \delta)/2$, while \hat{J}^2 and \hat{K}^2 are not diagonal in the Schwinger boson basis and so ℓ is found through explicit evaluation. This is related to an important point: in general, $|\ell, m_j, m_k\rangle \neq |j=\ell, m_j\rangle \otimes |k=\ell, m_k\rangle$. We know this is not the case because the state given in Eq. (4) may be fully described by the permutationally symmetric basis states, but it is clearly not of this form. Lastly, we can do an accounting of all the basis states. The quantum number ℓ can range from $\ell = N/2$ down to $\ell = 1/2$ or 0 for odd or even N , respectively, in steps of one: $\ell \in \{N/2, N/2 - 1, \dots, 0 \text{ or } 1/2\}$. Each ℓ has $2\ell + 1$ many values of m_j and m_k , with $m_j, m_k \in \{+\ell, +\ell - 1, \dots, -\ell\}$. This sum then gives the correct total number of states,

$$\sum_{\ell}^{N/2} (2\ell + 1)^2 = (N+1)(N+2)(N+3)/6. \quad (16)$$

C. Irreducible Representations of SU(2) Subgroups

As stated above, the basis states $|\ell, m_j, m_k\rangle$ are not trivially separable into wavefunctions of the J and K degrees of freedom. This is because each value ℓ corresponds to many different configurations of the atoms. Consider, for example, the

states $|\ell = \frac{3}{2}, m_j = \frac{1}{2}, m_k = \frac{1}{2}\rangle$ and $|\ell = \frac{1}{2}, m_j = \frac{1}{2}, m_k = \frac{1}{2}\rangle$ for $N = 3$. For $\ell = 3/2$, we have

$$\begin{aligned} \left| \frac{3}{2}, \frac{1}{2}, \frac{1}{2} \right\rangle &= \frac{1}{3} (|110\rangle_s + |101\rangle_s + |011\rangle_s) \\ &\otimes (|\uparrow\uparrow\downarrow\rangle_s + |\uparrow\downarrow\uparrow\rangle_s + |\downarrow\uparrow\uparrow\rangle_s), \end{aligned} \quad (17)$$

where the states on the right-hand-side of the equation are in the single-particle basis with the notation $|ijk\rangle_s = |i\rangle_1 |j\rangle_2 |k\rangle_3$. The $\ell = 1/2$ state is more complicated,

$$\begin{aligned} \left| \frac{1}{2}, \frac{1}{2}, \frac{1}{2} \right\rangle &= \frac{1}{3\sqrt{2}} (|110\rangle_s + e^{i2\pi/3} |101\rangle_s + e^{i4\pi/3} |011\rangle_s) \\ &\otimes (|\uparrow\uparrow\downarrow\rangle_s + e^{i2\pi/3} |\uparrow\downarrow\uparrow\rangle_s + e^{i4\pi/3} |\downarrow\uparrow\uparrow\rangle_s) \\ &+ \frac{1}{3\sqrt{2}} (-|110\rangle_s + e^{i\pi/3} |101\rangle_s + e^{i5\pi/3} |011\rangle_s) \\ &\otimes (-|\uparrow\uparrow\downarrow\rangle_s + e^{i\pi/3} |\uparrow\downarrow\uparrow\rangle_s + e^{i5\pi/3} |\downarrow\uparrow\uparrow\rangle_s). \end{aligned} \quad (18)$$

We therefore see that the state $|\ell = \frac{3}{2}, m_j = \frac{1}{2}, m_k = \frac{1}{2}\rangle$ has no algebraic entanglement between the two degrees of freedom whereas $|\ell = \frac{1}{2}, m_j = \frac{1}{2}, m_k = \frac{1}{2}\rangle$ has an algebraic entanglement entropy of 1 bit. We emphasize again that both states are still overall permutationally symmetric. This pattern will hold as N increases. In general, the N -particle bosonic irrep of SU(4) has every SU(2) \otimes SU(2) representation from $\ell = N/2$ down to $\ell = 1/2$ or 0 for N being odd or even, respectively. Upon tracing out one degree of freedom, each SU(2) irrep is identified by a specific value of ℓ and will have a multiplicity of d_N^ℓ given by [84]

$$d_N^\ell = \frac{N!(2\ell + 1)}{(\frac{N}{2} + \ell + 1)! (\frac{N}{2} - \ell)!}, \quad (19)$$

which represents the number of ‘‘copies’’ of the state in the single-particle basis that only differ by a permutation of atom indices (i.e., they are described by the same Young tableaux), and thus evolve identically under a permutationally symmetric Hamiltonian. Note that $d_N^{N/2} = 1$, as expected for the bosonic subspace.

We can now use the d_N^ℓ -fold multiplicity of each ℓ -irrep of SU(2) to establish the following result. If we trace out one of the degrees of freedom, say K , each basis state $|\ell, m_j, m_k\rangle$ is mapped to a density matrix with support over each of the d_N^ℓ -many orthogonal copies of the SU(2) irrep. Stated in an equation, this means that

$$\begin{aligned} \hat{\rho}_{\ell, m_j, m'_j} &= \text{Tr}_K \left(|\ell, m_j, m_k\rangle \langle \ell, m'_j, m_k| \right) \\ &= \frac{1}{d_N^\ell} \sum_{i=1}^{d_N^\ell} |\ell, m_j, i\rangle \langle \ell, m'_j, i|, \end{aligned} \quad (20)$$

where i is an extra quantum number (from outside the group) needed to distinguish each copy [25]. Notably, there are no coherences between different irreps of SU(2) in the reduced density matrix, and no coherences between different copies. For example, tracing out the K degree of freedom of Eq. (18)

would lead to $i = 1$ being the outer product of the state in the first line and $i = 2$ being the outer product of the state in the third line with no coherence between them. Similarly, if we were to trace over the J degree of freedom, we obtain

$$\begin{aligned} \hat{\rho}_{\ell, m_k, m'_k} &\equiv \text{Tr}_J (|\ell, m_j, m_k\rangle\langle\ell, m_j, m'_k|) \\ &= \frac{1}{d_N^\ell} \sum_{i=1}^{d_N^\ell} |\ell, m_k, i\rangle\langle\ell, m'_k, i|. \end{aligned} \quad (21)$$

With this, to solve for the algebraic entanglement entropy in general, we just have to decompose it into the constituent density matrices on the J and K degrees of freedom.

IV. AN ALGORITHM FOR ALGEBRAIC ENTANGLEMENT ENTROPY

With the structure of the state space in place and the multiplicity of the relevant subgroups worked out, we can now describe the structure of our algorithm for calculating algebraic entanglement entropy efficiently. It is conceptually the same for pure versus mixed states, but we will describe them separately. For pure states, the state vector can be described in $\mathcal{O}(N^3)$ coefficients, while mixed states require $\mathcal{O}(N^6)$ many coefficients to describe the density matrix. Of course, the use of sparse matrices can reduce the numerical complexity drastically for most systems.

It is helpful to imagine the states organized onto a three-dimensional grid, where each row is labeled by m_j , while each column is labeled by m_k , and where the third layer is labeled by ℓ . This organizes the states into a pyramid structure shown in Fig. 2(a), where $\text{SU}(2) \otimes \text{SU}(2)$ dynamics don't mix the layers of the pyramid (don't change ℓ), but $\text{SU}(4)$ dynamics in general can couple states on different layers. We show a picture of this for $N = 4$ in Fig. 2(a). The six generators of $\text{SU}(2) \otimes \text{SU}(2)$, given by $\hat{G}_{\mu I}$ and $\hat{G}_{I\mu}$ for $\mu \in \{x, y, z\}$, don't move a state between layers of this pyramid. The remaining $\text{SU}(4)$ operators, $\hat{G}_{\mu\nu}$ for $\mu, \nu \in \{x, y, z\}$, can change ℓ and therefore generate algebraic entanglement. This conclusion is equally clear from the definitions of Eq. (8), and is important for the steps of the algorithm. Moreover, our observation in the previous section about the multiplicity of the different ℓ layers leads to an important conclusion; basis states on layers $\ell \neq N/2$ are automatically endowed (when $N > 2$) with algebraic entanglement between J and K through the use of representation theory. This fact is the sole reason we can calculate a linearly scaled entanglement entropy, $S_E \sim N$, using a polynomial-scaled Hilbert space.

A. Pure State

We begin with the case that the system remains in a pure state $|\psi\rangle$. To calculate the algebraic entanglement entropy, one first has to find the state coefficients in the $|\ell, m_j, m_k\rangle$ basis to take advantage of the innate symmetry. For each $|\ell, m_j, m_k\rangle$,

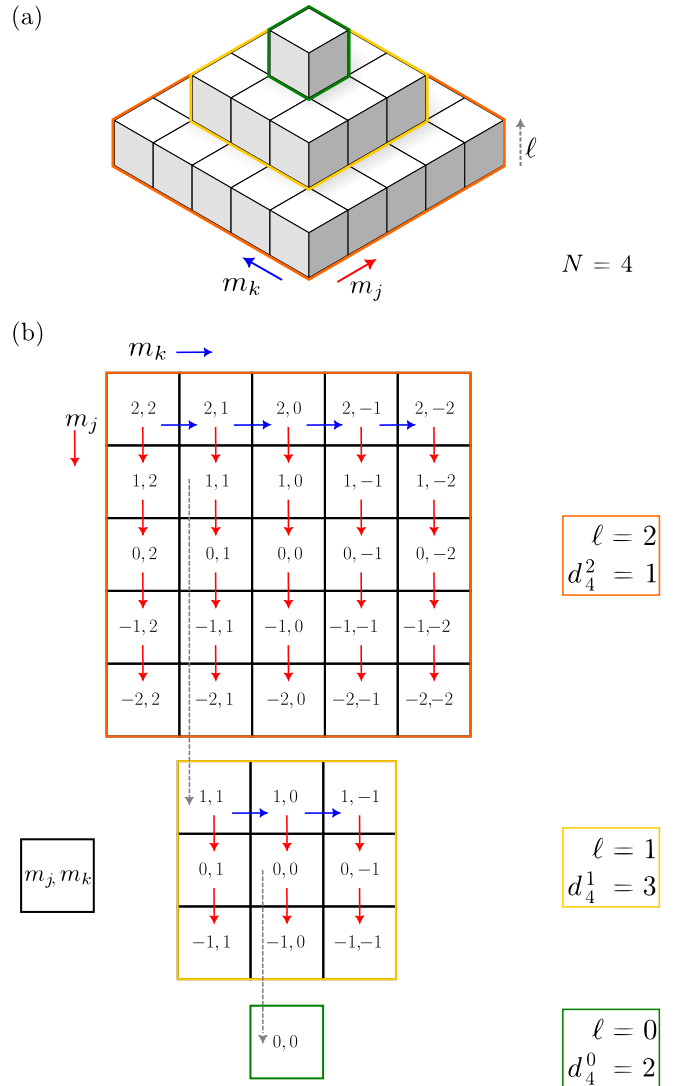


FIG. 2. (a) The state pyramid for $N = 4$. (b) The layers of the state pyramid, where each ℓ corresponding to one of the irreducible representations of $\text{SU}(2) \otimes \text{SU}(2)$. Red arrows indicate an application of \hat{J}_- , blue arrows indicate an application of \hat{K}_- , and gray arrows indicate a Gram-Schmidt orthogonalization step. The ℓ label and the multiplicity d_N^ℓ are given to the right of each layer.

we need to calculate the coefficients

$$p_{\ell, m_j, m_k} = \langle \ell, m_j, m_k | \psi \rangle. \quad (22)$$

Of course, one could simply simulate the state dynamics in this basis, but since the Schwinger boson basis Eq. (9) is typically used, we will assume the state dynamics $|\psi(t)\rangle$ are simulated in the Schwinger boson basis and one wants to calculate the p_{ℓ, m_j, m_k} coefficients as the state evolves. To do so algorithmically, we start with the state coefficients

$$|\psi\rangle = c_{\alpha, \beta, \gamma, \delta} |\alpha, \beta, \gamma, \delta\rangle. \quad (23)$$

In this basis, we can first identify the state $|\ell = N/2, m_j = N/2, m_k = N/2\rangle = |N, 0, 0, 0\rangle$. In principle,

one could start in any preferred basis (e.g., Ref. [67]) so long as one can identify the state $|\ell = N/2, m_j = N/2, m_k = N/2\rangle$. We know that N applications of \hat{J}_- on this state will produce $|\ell = N/2, m_j = -N/2, m_k = N/2\rangle$, while N applications of \hat{K}_- will produce $|\ell = N/2, m_j = N/2, m_k = -N/2\rangle$. As a result, we can iterate over the $\ell = N/2$ states using \hat{J}_- and \hat{K}_- , whereupon

$$P_{\frac{N}{2}, m_j, m_k} = \left\langle \frac{N}{2}, \frac{N}{2}, \frac{N}{2} \left| \frac{(\hat{J}_+)^{\frac{N}{2}-m_j} (\hat{K}_+)^{\frac{N}{2}-m_k}}{\mathcal{N}_{\frac{N}{2}, m_j, m_k}} \right| \psi \right\rangle, \quad (24)$$

where $\mathcal{N}_{\ell, m_j, m_k}$ is a normalization factor after the raising operators are applied.

In order to generate the states of $\ell = \frac{N}{2} - 1$, we use the state $|N/2, N/2 - 1, N/2 - 1\rangle$ and Gram-Schmidt orthogonalization [85, 86] to find $|N/2 - 1, N/2 - 1, N/2 - 1\rangle$ such that

$$\left\langle \frac{N}{2}, \frac{N}{2} - 1, \frac{N}{2} - 1 \left| \frac{N}{2} - 1, \frac{N}{2} - 1, \frac{N}{2} - 1 \right\rangle = 0. \quad (25)$$

We can then generate the next ‘‘layer’’ of state coefficients using

$$P_{\frac{N}{2}-1, m_j, m_k} = \left\langle \frac{N}{2} - 1, \ell, \ell \left| \frac{(\hat{J}_+)^{\ell-m_j} (\hat{K}_+)^{\ell-m_k}}{\mathcal{N}_{\ell, m_j, m_k}} \right| \psi \right\rangle. \quad (26)$$

This process is repeated for each value of ℓ , where the n^{th} layer is found via Gram-Schmidt orthogonalization using the $n - 1$ states sharing the same m_j and m_k , but differing in ℓ . This iterative process to find all the state coefficients p_{ℓ, m_j, m_k} is shown pictorially in Fig. 2(b), where the red arrows depict \hat{J}_- operations, the blue arrows depict \hat{K}_- operations, and the gray arrows depict the Gram-Schmidt orthogonalization steps.

It is now a straightforward process to trace out one of the degrees of freedom, say K . We use Eq. (20) to find

$$\begin{aligned} \hat{\rho}_J &= \text{Tr}_K(|\psi\rangle\langle\psi|) \\ &= \sum_{\ell}^{N/2} \left[\sum_{m_j, m'_j, m_k = -\ell}^{\ell} P_{\ell, m_j, m_k} P_{\ell, m'_j, m_k}^* \hat{\rho}_{\ell, m_j, m'_j} \right], \quad (27) \end{aligned}$$

where the sum on ℓ starts at 0 or 1/2 for even or odd N , respectively. We can use this form because $\hat{\rho}_J$ will never support coherences between layers of differing ℓ . A similar equation for $\hat{\rho}_K$ is found when tracing out the other degree of freedom. Now, we may simply diagonalize each layer one-by-one to find the eigenvalues of $\hat{\rho}_J$. We do this by constructing the matrix

$$\mathbf{M}^{(\ell)} = \sum_{m_j, m'_j, m_k = -\ell}^{\ell} P_{\ell, m_j, m_k} P_{\ell, m'_j, m_k}^* \mathbf{E}_{m_j+\ell, m'_j+\ell}^{(\ell)}, \quad (28)$$

where $\mathbf{E}_{\mu\nu}^{(\ell)}$ is a $(2\ell + 1) \times (2\ell + 1)$ matrix with a 1 in the μ^{th} row and ν^{th} column, and zeros everywhere else. Therefore, $\mathbf{M}^{(\ell)}$ is the matrix whose elements are populated by each $P_{\ell, m_j, m_k} P_{\ell, m'_j, m_k}^*$ coefficient. Diagonalizing this matrix yields the eigenvalues for the ℓ^{th} component of $\hat{\rho}_J$. Defining $\lambda_i^{(\ell)}$ to

be the i^{th} eigenvalue of $\mathbf{M}^{(\ell)}$, we must remember that there are d_N^{ℓ} -many copies of the eigenvalue $\lambda_i^{(\ell)}/d_N^{\ell}$ in the full spectrum of $\hat{\rho}_J$ due to the multiplicity of the given irrep.

Lastly, the algebraic entanglement entropy of $\hat{\rho}_J$ may be directly calculated by summing over the eigenvalues of each $\mathbf{M}^{(\ell)}$ and including the proper d_N^{ℓ} -fold degeneracy of these eigenvalues,

$$\begin{aligned} S_E(\hat{\rho}_J) &= \text{Tr}_J[\hat{\rho}_J \ln(\hat{\rho}_J)] \\ &= - \sum_{\ell}^{N/2} \left[\sum_{i=0}^{2\ell+1} \lambda_i^{(\ell)} \ln \left(\frac{\lambda_i^{(\ell)}}{d_N^{\ell}} \right) \right], \quad (29) \end{aligned}$$

where we take $0 \times \ln(0) = 0$ for any zero eigenvalues. We note that each $\lambda_i^{(\ell)}/d_N^{\ell}$ appears d_N^{ℓ} -many times, which is why the first occurrence of $\lambda_i^{(\ell)}$ in Eq. (29) doesn't have an accompanying d_N^{ℓ} . We again emphasize the role of the multiplicity of the $\text{SU}(2)$ irreps to accurately calculate the algebraic entanglement entropy. For example, consider $|\psi\rangle = |1/2, 1/2, 1/2\rangle$ for $N = 3$ which we wrote in the single-particle basis in Eq. (18). Since the state is purely in a single basis state, we have a single nonzero eigenvalue $\lambda_1^{(1/2)} = 1$ which one would often think indicates zero entropy. However, the multiplicity of $d_3^{1/2} = 2$ in Eq. (29) corrects this and gives $S_E(\hat{\rho}_J) = \ln(2) = 1$ bit, which agrees with what we found in Eq. (18).

The pure state algorithm presented above is summarized in pseudocode in Algorithm 1. There, we show algorithmically how to start with a state $|\psi\rangle$ in the Schwinger boson basis for a given N and calculate the entanglement entropy for $\hat{\rho}_J$ and $\hat{\rho}_K$.

B. Mixed State

We now describe how to use the above procedure for mixed states. In general, this requires $O[\dim(\mathcal{H})^2] = O(N^6)$ many coefficients to describe the density matrix $\hat{\rho}$. However, the algorithm is effectively the same for calculating $\hat{\rho}_J$ and $\hat{\rho}_K$. The only non-trivial change is that we will have coefficients that depend on two copies of ℓ, m_j , and m_k :

$$P_{\ell, m_j, m_k}^{\ell', m'_j, m'_k} = \langle \ell, m_j, m_k | \hat{\rho} | \ell', m'_j, m'_k \rangle. \quad (30)$$

If $\hat{\rho}$ were a pure state, it is straightforward to see that $P_{\ell, m_j, m_k}^{\ell', m'_j, m'_k} = P_{\ell, m_j, m_k} P_{\ell', m'_j, m'_k}^*$ from Eq. (22). This means that, for general mixed states, one must iterate over two sets of states, $|\ell, m_j, m_k\rangle$ and $|\ell', m'_j, m'_k\rangle$, to calculate all values of $P_{\ell, m_j, m_k}^{\ell', m'_j, m'_k}$.

Once these coefficients are calculated, we can express any general density matrix, $\hat{\rho}$, using the pyramid structure:

$$\hat{\rho} = \sum_{\ell, \ell'}^{N/2} \sum_{\mathbf{m}} P_{\ell, m_j, m_k}^{\ell', m'_j, m'_k} |\ell, m_j, m_k\rangle \langle \ell', m'_j, m'_k|. \quad (31)$$

where $\mathbf{m} = m_j, m_k, m'_j, m'_k$ for legibility, and the sums over m_j, m_k run from $-\ell$ to $+\ell$, while the sums over m'_j, m'_k run

```

Begin with a state  $|\psi\rangle$  in  $|\alpha, \beta, \gamma, \delta\rangle$  basis;
Initialize  $\hat{J}_-$  and  $\hat{K}_-$  in  $|\alpha, \beta, \gamma, \delta\rangle$  basis;
 $\ell_{\min} \leftarrow \text{mod}[N, 2]/2$ ;
 $S_J \leftarrow 0$ ;
 $S_K \leftarrow 0$ ;
for  $\ell = \frac{N}{2} : -1 : \ell_{\min}$  do
   $\mathbf{p}_\ell \leftarrow \text{zeros}(2\ell + 1, 2\ell + 1)$ ;
  if  $\ell = \frac{N}{2}$  then
     $|s'\rangle \leftarrow |N, 0, 0, 0\rangle$ ;
  else
    Gram-Schmidt orthogonalization for  $|s'\rangle$ ;
  end
  for  $j = 1 : 2\ell + 1$  do
     $|s\rangle \leftarrow |s'\rangle$ ;
     $\mathbf{p}_\ell(j, 1) \leftarrow \langle s|\psi\rangle$ ;
    for  $k = 2 : 2\ell + 1$  do
       $|s\rangle \leftarrow \hat{K}_- |s\rangle$ ;
      Normalize  $|s\rangle$ ;
       $\mathbf{p}_\ell(j, k) \leftarrow \langle s|\psi\rangle$ ;
    end
     $|s'\rangle \leftarrow \hat{J}_- |s\rangle$ ;
    Normalize  $|s'\rangle$ ;
  end
   $d_N^\ell \leftarrow N!(2\ell + 1)/[(N/2 + \ell + 1)!(N/2 - \ell)!]$ ;
   $\mathbf{M}_J^{(\ell)}(j, j') \leftarrow \sum_{k=0}^{2\ell+1} \mathbf{p}_\ell(j, k)\mathbf{p}_\ell^*(j', k)$ ;
   $\mathbf{M}_K^{(\ell)}(k, k') \leftarrow \sum_{j=0}^{2\ell+1} \mathbf{p}_\ell(j, k)\mathbf{p}_\ell^*(j, k')$ ;
   $\lambda_J \leftarrow \text{eigenvalues}(\mathbf{M}_J^{(\ell)})$ ;
   $\lambda_K \leftarrow \text{eigenvalues}(\mathbf{M}_K^{(\ell)})$ ;
   $S_J \leftarrow S_J - \sum_{j=0}^{2\ell+1} \lambda_J(j) \ln(\lambda_J(j)/d_N^\ell)$ ;
   $S_K \leftarrow S_K - \sum_{k=0}^{2\ell+1} \lambda_K(k) \ln(\lambda_K(k)/d_N^\ell)$ ;
end

```

Algorithm 1: The algorithm for finding the algebraic entanglement entropy of pure state $|\psi\rangle$. The algorithm loops over each “layer” of states for one value of ℓ ranging from $N/2$ down to either $1/2$ or 0 . The starting state for layer ℓ is found by Gram-Schmidt orthogonalization using all previous states that have $m_j = m_k = \ell$. From this starting state, all other states are reached in the layer by repeated application of \hat{J}_- and \hat{K}_- . These states are used to calculate the state coefficients of $|\psi\rangle$, and subsequently construct the matrix \mathbf{M} . Lastly, the eigenvalues of this matrix and the multiplicity d_N^ℓ are used to calculate the entanglement entropy.

from $-\ell'$ to $+\ell'$. The rest of the procedure is the same as for pure states because we know $\hat{\rho}_J$ and $\hat{\rho}_K$ will have no coherence between differing values of ℓ and ℓ' . Therefore, we have

$$\begin{aligned} \hat{\rho}_J &= \text{Tr}_K(\hat{\rho}) \\ &= \sum_{\ell}^{N/2} \left[\sum_{m_j, m'_j, m_k} P_{\ell, m_j, m_k}^{\ell, m'_j, m_k} \hat{\rho}_{\ell, m_j, m'_j} \right], \end{aligned} \quad (32)$$

where m_j, m'_j, m_k are summed from $-\ell$ to ℓ . This agrees with the pure state case Eq. (20), and we can find a similar equation for $\hat{\rho}_K$.

Once again, we diagonalize each layer for distinct ℓ one-by-one to find the eigenvalues of $\hat{\rho}_J$. We do this by constructing

the matrix

$$\mathbf{M}^{(\ell)} = \sum_{m_j, m'_j, m_k = -\ell}^{\ell} P_{\ell, m_j, m_k}^{\ell, m'_j, m_k} \mathbf{E}_{m_j + \ell, m'_j + \ell}^{(\ell)}. \quad (33)$$

Diagonalizing this matrix yields the eigenvalues for the ℓ^{th} component of $\hat{\rho}_J$. The algebraic entanglement entropy of $\hat{\rho}_J$ may then be directly calculated in an equivalent manner to Eq. (29). For mixed states, however, we note that $S_E(\hat{\rho}_J) \neq S_E(\hat{\rho}_K)$ as the system may also be entangled to an external environment. The algorithm for mixed states presented above is summarized in pseudocode in Algorithm 2.

```

Begin with a state  $\hat{\rho}$  in  $|\alpha, \beta, \gamma, \delta\rangle$  basis;
Initialize  $\hat{J}_-$  and  $\hat{K}_-$  in  $|\alpha, \beta, \gamma, \delta\rangle$  basis;
 $\ell_{\min} \leftarrow \text{mod}[N, 2]/2$ ;
 $S_J \leftarrow 0$ ;
for  $\ell = \frac{N}{2} : -1 : \ell_{\min}$  do
   $s_a \leftarrow \text{Empty}(2\ell + 1) \times (2\ell + 1)$  array;
  if  $\ell = \frac{N}{2}$  then
     $|s'\rangle \leftarrow |N, 0, 0, 0\rangle$ ;
  else
    Gram-Schmidt orthogonalization for  $|s'\rangle$ ;
  end
  for  $j = 1 : 2\ell + 1$  do
     $|s\rangle \leftarrow |s'\rangle$ ;
     $s_a(j, 1) = |s\rangle$ ;
    for  $k = 2 : 2\ell + 1$  do
       $|s\rangle \leftarrow \hat{K}_- |s\rangle$ ;
      Normalize  $|s\rangle$ ;
       $s_a(j, k) = |s\rangle$ ;
    end
     $|s'\rangle \leftarrow \hat{J}_- |s\rangle$ ;
    Normalize  $|s'\rangle$ ;
  end
   $P \leftarrow \text{zeros}(2\ell + 1, 2\ell + 1)$ ;
  for  $j, j', k = 1 : 2\ell + 1$  do
     $P(j, j', k) \leftarrow s_a(j, k)^\dagger \hat{\rho} s_a(j', k)$ ;
  end
   $\mathbf{M}_J^{(\ell)} \leftarrow \text{zeros}(2\ell + 1, 2\ell + 1)$ ;
  for  $j, j' = 1 : 2\ell + 1$  do
     $\mathbf{M}_J^{(\ell)}(j, j') \leftarrow \sum_{k=0}^{2\ell+1} P(j, j', k)$ ;
  end
   $\lambda_J \leftarrow \text{eigenvalues}(\mathbf{M}_J^{(\ell)})$ ;
   $d_N^\ell \leftarrow N!(2\ell + 1)/[(N/2 + \ell + 1)!(N/2 - \ell)!]$ ;
   $S_J \leftarrow S_J - \sum_{j=0}^{2\ell+1} \lambda_J(j) \ln(\lambda_J(j)/d_N^\ell)$ ;
end

```

Algorithm 2: The algebraic entanglement entropy algorithm for the spin degree of freedom J of a mixed state $\hat{\rho}$. Similar to Algorithm 1, the starting state for layer ℓ is found by Gram-Schmidt orthogonalization using all previous states that have $m_j = m_k = \ell$. For the momentum degree of freedom K , the for loop over j, j', k becomes a for loop over k, k', j , the for loop over j, j' becomes a for loop over k, k' , and the sums $\sum_{j=0}^{2\ell+1}$ become $\sum_{k=0}^{2\ell+1}$.

For mixed states, the entanglement entropy of just $\hat{\rho}_J$ or $\hat{\rho}_K$ is often not very illuminating as it could simply indicate entanglement between the degrees of freedom and an external

environment rather than algebraic entanglement between the two degrees of freedom. However, our algorithm allows us to calculate any other quantities depending on the spectrum of $\hat{\rho}_J$ and $\hat{\rho}_K$. In particular, we can calculate the coherent information [87],

$$\begin{aligned} I(J)K &= S_E(\hat{\rho}_K) - S_E(\hat{\rho}), \\ I(K)J &= S_E(\hat{\rho}_J) - S_E(\hat{\rho}), \end{aligned} \quad (34)$$

which we note is the negative of the conditional entropy [88, 89]. Therefore, the coherent information provides a condition for state transfer whose conventional explanation (from Ref. [89]) goes as follows. Imagine there are two parties, J and K . Party J has access to the full $\hat{\rho}$ while party K only has access to $\hat{\rho}_K$. A negative $I(J)K$ can be understood as the number of quantum bits that party J must send to K in order to achieve state transfer. If it is positive, however, then the sender and receiver gain access to additional quantum resources after state transfer. Put more simply, coherent information measures quantum correlations in a similar way as mutual information measures classical correlations [87]. Therefore, the positivity of Eq. (34) provides a sufficient condition for algebraic entanglement in mixed states [88, 89]. Interpreted in the context of motional and internal degrees of freedom, this means directly teleportating the internal state of the atoms onto their momentum degree of freedom is possible [29], in principle.

V. EXAMPLES

We will now calculate the algebraic entanglement entropy for four example physical systems. First, we will calculate the algebraic entanglement entropy for the spin and momentum degrees of freedom for a state evolved under Eq. (2) and compare the algorithm to the analytical solution from Sec. II. Second, we will revisit the example of Refs. [1, 57] and compare the algorithm to a simulation using the full 4^N dynamics. Third, we will introduce decoherence into the model from Refs. [1, 57], where the loss is caused by a leaky cavity. Lastly, we will calculate the relevant entropy dynamics for a model with dynamics driven by solely decoherence from our companion paper, Ref. [67]. The last three examples, Secs. VB-VD, all require a clever application of representation theory in order to simulate anything more than a few particles. In all four examples, we let the spin degree of freedom correspond to J while momentum corresponds to K .

A. Illustrative Example, Revisited.

We will start with the illustrative example from Sec. II. We see Eq. (2) has the form of the operators given in Eq. (8), namely,

$$\hat{H}_{\text{IE}} = \frac{\hbar\Delta}{2}\hat{G}_{zI} + \frac{\hbar\Omega}{2}\hat{G}_{xx}. \quad (35)$$

From Eq. (3), we can find the algebraic entanglement entropy analytically. For sake of simplicity, we will once again consider the limit of zero detuning, $\Delta = 0$, where the algebraic

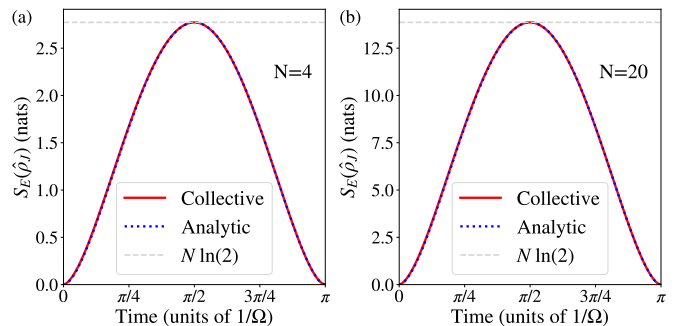


FIG. 3. The algebraic entanglement entropy for the collective internal states (corresponding to J) of the atoms for the Hamiltonian in Eq. (35). (a) shows results for $N = 4$ while (b) shows results for $N = 20$. We display the numerical results (red lines) and the analytical results from Eq. (36) (blue lines). In both plots, we see that the entanglement entropy grows to the maximum possible value of $N \ln(2)$ (gray lines) given in Eq. (6) at $t = \pi/(2\Omega)$. We find that the results from Algorithm 1 for the algebraic entanglement entropy follows the analytical solutions exactly.

entanglement entropy is given by

$$\begin{aligned} S_E(\hat{\rho}_J) &= -N \cos^2\left(\frac{\Omega t}{2}\right) \ln\left[\cos^2\left(\frac{\Omega t}{2}\right)\right] \\ &\quad - N \sin^2\left(\frac{\Omega t}{2}\right) \ln\left[\sin^2\left(\frac{\Omega t}{2}\right)\right], \end{aligned} \quad (36)$$

and $S_E(\hat{\rho}_K) = S_E(\hat{\rho}_J)$. To compare with Algorithm 1, we evolve the system from its initial state numerically and calculate the algebraic entanglement entropy using the steps outlined in Sec. IV. The results are shown in Fig. 3.

In Fig. 3, we see that an algorithm that uses a Hilbert space that grows polynomially with N can still accurately calculate an entanglement entropy which grows proportional to N rather than with $\ln(N)$. This is only possible because we have utilized the multiplicity d_N^{ℓ} of the irreps of $SU(2)$. This is interesting because it shows that these $SU(4)$ dynamics are efficiently simulatable in a polynomial-scaled space, and the dynamics can generate states with algebraic entanglement entropy growing faster than the dimension of the Hilbert space. In other words, the algebraic entanglement within the basis states allows algebraic entanglement entropy growth faster than $\ln[\dim(\mathcal{H}_{\text{sym}})]$, which is what one would expect from a maximally mixed state whose eigenvalues are $1/\dim(\mathcal{H}_{\text{sym}})$.

B. BOAT model

We now revisit the Hamiltonian presented in Refs. [1, 57], dubbed the beyond one-axis twisting (BOAT) model. Here, both interparticle entanglement and algebraic entanglement are generated, which makes analytical calculations used in the previous example no longer tractable. The Hamiltonian is given by

$$\hat{H}_{\text{BOAT}} = \hbar\chi\hat{G}_{(+x)}\hat{G}_{(-x)}, \quad (37)$$

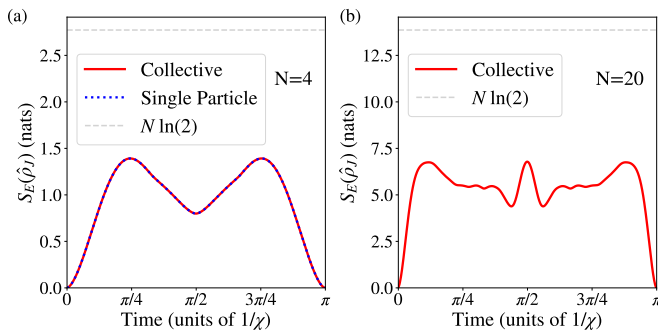


FIG. 4. The algebraic entanglement entropy for the collective internal states (corresponding to J) of the atoms for the BOAT Hamiltonian Eq. (37). (a) shows results for $N = 4$. Here, we can simulate the dynamics in the full single-particle basis and calculate the algebraic entanglement entropy (blue line), where we find it exactly matches the collective simulation (red line). (b) shows results for $N = 20$. Here, simulating the full 4^N dynamics is infeasible. However, the algorithm which runs on the $\mathcal{O}(N^3)$ state space still calculates the algebraic entanglement entropy efficiently.

which corresponds to a one-axis-twisting Hamiltonian [90] with the additional complication that the atoms have two momentum states. This Hamiltonian can be accomplished by a particle beam traversing a dispersive cavity while energy requirements limits the particles momenta along the cavity axis to $\pm\hbar k/2$ [57]. After adiabatically eliminating the cavity field, we arrive at the atom-only nonlinear Hamiltonian in Eq. (37). The nonlinearity in this model will generate interparticle entanglement while the structure of the operators will generate algebraic entanglement, the combination of which allows for multi-parameter estimation beyond the standard quantum limit [1]. Since the Hamiltonian is described fully by collective SU(4) operators, the dynamics can be characterized by the states presented in Sec. II. We assume the atoms are initially in a superposition of the ground and excited state with a momenta of $-\hbar k/2$,

$$|\Psi(0)\rangle = \bigotimes_{j=1}^N \left(\left[\frac{|0\rangle_j + |1\rangle_j}{\sqrt{2}} \right] \otimes |\downarrow\rangle_j \right). \quad (38)$$

We can evolve the system using the Schrödinger equation and calculate the algebraic entanglement entropy $S_E(\hat{\rho}_J) = S_E(\hat{\rho}_K)$. The numerical results for the dynamics of the algebraic entanglement entropy for $N = 4$ are shown in Fig. 4(a). In order to benchmark the algorithm, we also simulate dynamics in the full 4^N single-particle basis. We find perfect agreement between the two results.

We take a moment to highlight an interesting fact. If we were to calculate an entanglement witness such as the quantum Fisher information for \hat{G}_{xI} , as is done in Ref. [57], we would find that there is a large amount of interparticle entanglement. Despite this, we see that there is less algebraic entanglement than in the previous example shown in Sec. V A. In fact, we can see from the structure of the Hamiltonian in Eq. (35) and its solutions that there is no interparticle entanglement whatsoever in the previous example, despite there being a large amount of algebraic entanglement, which is how we are able to easily find

analytical solutions to the previous example. This is no longer the case for the BOAT model, and so the results of Fig. 4(b) for $N = 20$ would not be possible without the polynomial-scaling of Algorithm 1. Therefore, we are able to efficiently perform a calculation in Fig. 4(b) that would typically require a $4^{20} \sim 10^{12}$ dimensional Hilbert space.

C. Leaky BOAT Model

We now introduce an additional complication not included in the BOAT model in Refs. [1, 57], which we use to highlight the need to calculate coherent information in the case of open quantum systems. If the decay of the cavity field into free space were included in the model of Ref. [57], one would find this corresponds to a decoherence jump operator that goes as $\hat{L}_d = \sqrt{\Gamma_c} \hat{G}_{(-)x}$ after adiabatically eliminating the cavity field, similar to Ref. [67]. Here, time dynamics are dictated by the Born-Markov master equation,

$$\frac{\partial \hat{\rho}}{\partial t} = \hat{\mathcal{L}}_{\text{BOAT}} \hat{\rho} = -\frac{i}{\hbar} [\hat{H}_{\text{BOAT}}, \hat{\rho}] + \hat{\mathcal{D}}[\hat{L}_d] \hat{\rho}, \quad (39)$$

where $\hat{\mathcal{L}}_{\text{BOAT}}$ is the Liouvillian superoperator, \hat{H}_{BOAT} is the Hamiltonian from Eq. (37), and the Lindblad superoperator is given by

$$\hat{\mathcal{D}}[\hat{O}] \hat{\rho} = \hat{O} \hat{\rho} \hat{O}^\dagger - (\hat{O}^\dagger \hat{O} \hat{\rho} + \hat{\rho} \hat{O}^\dagger \hat{O})/2. \quad (40)$$

We simulate the dynamics for this model using the same starting state given by Eq. (38) and three values of decoherence, $\Gamma_c = 0.05\chi$, $\Gamma_c = 0.25\chi$, and $\Gamma_c = 0.5\chi$, shown in Figs. 5(a), (b), and (c), respectively. For these dynamics, we also use Eq. (34) to calculate the coherent information between the two degrees of freedom to demonstrate algebraic entanglement. As expected, we find that the general features of the closed system in Fig. 4, namely the three ‘‘humps’’ where the entanglement entropy spikes to its maximum value in Fig. 4(b), decay away as the decay rate Γ_c increases compared to the squeezing rate χ . Moreover, Fig. 5(a) demonstrates the importance of studying the coherent information rather than just the entanglement entropy when studying open quantum systems. We see that maximum value of the three ‘‘humps’’ in the entanglement entropy increases as time increases, but ‘‘humps’’ in the coherent information decreases as time increases. This indicates that the algebraic entanglement between the two degrees of freedom is decreasing as the entanglement of the total system with the environment is increasing over the dynamics.

Lastly, we examine the entropies and coherent information of the model at steady-state, $\hat{\mathcal{L}}_{\text{BOAT}} \hat{\rho}_{\text{ss}} = 0$, as a function of χ and Γ_c . To find the state which Eq. (38) relaxes into, we simply simulate the dynamics for a long time $\hat{\rho}_{\text{ss}} = \hat{\rho}(t \rightarrow \infty)$. The results are shown in Fig. 6. We see that the steady-state entropy on the K degree of freedom is fixed regardless of Γ_c and χ even though it varies during the dynamics [Fig. 5]. On the J degree of freedom, however, we see that steady-state entropy decreases as the ratio Γ_c/χ goes from below one to above one. The fixed entropy of the K degree of freedom in steady-state is a result of the fact that both \hat{H}_{BOAT} and \hat{L}_d

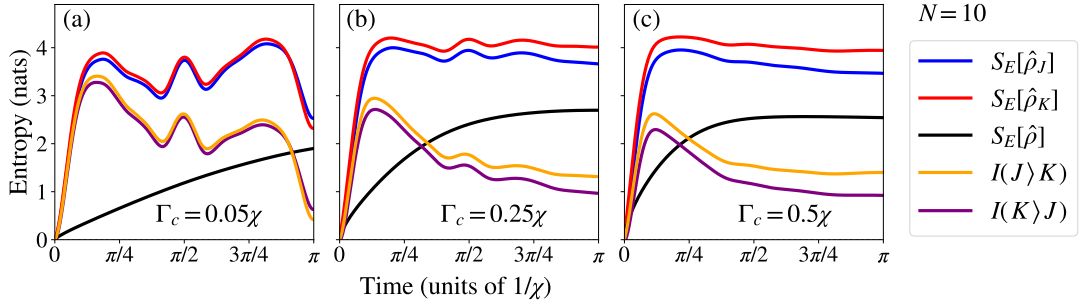


FIG. 5. Results for the leaky BOAT model Eq. (39). We display the algebraic entanglement entropy for $\hat{\rho}_J$ (blue) and $\hat{\rho}_K$ (red), the entropy for the total state $\hat{\rho}$ (black), and the coherent informations for $I(J)K$ (orange) and $I(K)J$ (purple). The parameters are (a) $\Gamma_c = 0.05\chi$, (b) $\Gamma_c = 0.25\chi$, and (c) $\Gamma_c = 0.5\chi$. In all three, we see that both $I(J)K$ and $I(K)J$ are positive, indicating the presence of algebraic entanglement between J and K . For larger decay rates, we see that the entanglement entropy of $\hat{\rho}_J$ and $\hat{\rho}_K$ differ due to entanglement with the environment, which is indicated by the growing entropy of $\hat{\rho}$.

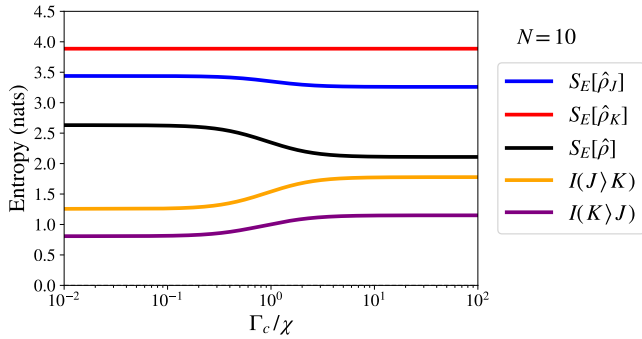


FIG. 6. The steady-state of the leaky BOAT model Eq. (39) as a function of Γ_c/χ . We again plot the algebraic entanglement entropy for $\hat{\rho}_J$ (blue) and $\hat{\rho}_K$ (red), the entropy for the entire $\hat{\rho}$ (black), and the coherent informations $I(J)K$ (orange) and $I(K)J$ (purple). We see that, even when photon loss dominates dynamics ($\Gamma_c \gg \chi$), we still find positive coherent information indicating usable algebraic entanglement.

commute with the operator $\hat{E}^2 \equiv \hat{G}_{(+x)}\hat{G}_{(-x)} + \hat{G}_{zI}^2 - \hat{G}_{zI}$, meaning a strong symmetry is present in the Liouvillian [91–93]. This symmetry corresponds to the Casimir operator for the $\mathfrak{su}(2)$ sub-algebra $\{\hat{G}_{zI}, \hat{G}_{(+x)}, \hat{G}_{(-x)}\}$, which fixes the steady state dynamics for K based on the starting state. The entropy of the J degree of freedom in steady state, meanwhile, changes because the Hamiltonian effectively “re-pumps” the atoms, thereby allowing more entanglement to be generated with the environment via emission. This means each atom is near the equator of the J -Bloch sphere and, in terms of Fig. 2 (b), the density matrix will have support across multiple rows of m_j .

D. Spin-Momentum Superradiance

As a final example, we consider the dual superradiance system from Ref. [67] as an example of a fully dissipative system that generates algebraic entanglement between J and K .

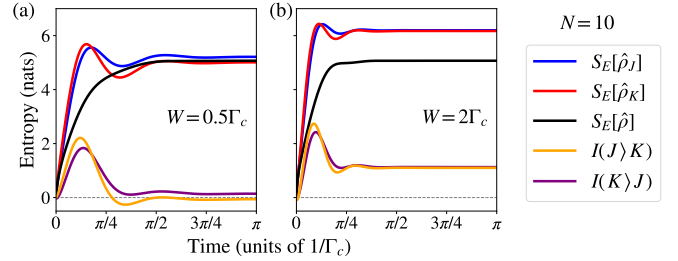


FIG. 7. The dynamics of the spin-momentum superradiance system from Eq. (41). We display the algebraic entanglement entropy for $\hat{\rho}_J$ (blue) and $\hat{\rho}_K$ (red), the entropy for the entire $\hat{\rho}$ (black), and the coherent informations $I(J)K$ (orange) and $I(K)J$ (purple). The parameters are (a) $W = 0.5\Gamma_c$ and (b) $W = 2\Gamma_c$.

This model begins with the leaky BOAT Liouvillian Eq. (39) that is on resonance, such that $\chi = 0$, mediated by a bad-cavity along the x -axis. A second bad-cavity along the z -axis and a classical drive can mediate a two-photon Raman transition between the two internal states mediated by an auxiliary excited state [67, 94]. This leads to collective pumping from ground to excited state at a rate W without changing the momentum in the x -direction, such that the jump operator is $\hat{L}_r = \sqrt{W}\hat{G}_{(+x)}$. The master equation is thus

$$\frac{\partial \hat{\rho}}{\partial t} = \hat{\mathcal{L}}_{\text{SMS}}\hat{\rho} = \hat{\mathcal{D}}[\hat{L}_d]\hat{\rho} + \hat{\mathcal{D}}[\hat{L}_r]\hat{\rho}, \quad (41)$$

which, notably, has no unitary dynamics. We once again consider the atoms starting in the state given by Eq. (38). However, it is important to note that this state leads to the same steady state as the one considered in Ref. [67], $|\Psi'(0)\rangle = \bigotimes_j^N (|0\rangle_j \otimes |\downarrow\rangle_j)$, although the dynamics may be slightly different, because both initial states are in the same $U(1)$ subgroup.

We simulate the dynamics of the various entropy quantities for $W = \Gamma_c/2$ and $W = 2\Gamma_c$, which are shown in Fig. 7 (a) and (b), respectively. We see that the algebraic entanglement entropy for J and K each initially grow faster than the total entropy, meaning we initially find a positive coherent infor-

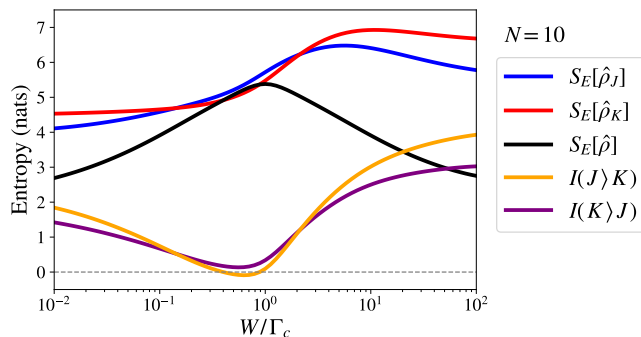


FIG. 8. The steady-state entropies of the spin-momentum superradiance system of Eq. (41) as a function of W/Γ_c . We see that fully dissipative dynamics still create large positive coherent information, and thus algebraic entanglement between J and K .

mation for both degrees of freedom and values of Γ_c . This suggests that dissipative engineering of these systems with $SU(4)$ symmetry provide powerful quantum information processing platforms. Surprisingly, we find that the case of a larger incoherent pump rate, $W = 2\Gamma_c$, generates more coherent information at steady-state than that of a lower incoherent pump rate, $W = \Gamma_c/2$. This is because the higher pump rate allows the system to relax into a state with population spread across the multiple ℓ layers of the pyramid.

We now examine the entropy quantities at steady-state, $\hat{\mathcal{L}}_{\text{SMS}}\hat{\rho}_{\text{ss}} = 0$, as a function of W compared to Γ_c . To find the state which Eq. (38) relaxes into, we again simulate the dynamics for a long time $\hat{\rho}_{\text{ss}} = \hat{\rho}(t \rightarrow \infty)$. The results are shown in Fig. 8. There, we see a more complicated response of the coherent information to the ratios of the re-pump and decay rates. The operator $\hat{E}^2 = \hat{G}_{(+)\ell}\hat{G}_{(-)\ell} + \hat{G}_{zI}^2 - \hat{G}_{zI}$ does not commute with $\hat{G}_{(+)\ell}$, and therefore we see the entropy on K differ as we adjust the rates. For the value $W = \Gamma_c$, we see that the system reaches its maximum entanglement with the environment, with both the entropy of the J and K degrees of roughly that of the total entropy. For both $W > \Gamma_c$, and $W < \Gamma_c$, we see that the coherent information grows, while the total entropy of the system decreases. Using the steady-state results presented in Ref. [67], we can gain insight into the algebraic entanglement generated in the system. Namely, in the case $W \gg \Gamma_c$, one finds that the steady-state dipole length of J becomes minuscule, $\langle \hat{j}^2 \rangle_{\text{ss}} \ll (N/2)(N/2 + 1)$ and so $j \ll N/2$. Since $\ell = j = k$, this indicates that there are $(N/2 - \ell) \gg 1$ many singlet pairs in both the J and K degrees of freedom, and so the basis states of $|\ell, m_j, m_k\rangle$ that are populated are endowed with a massive amount of algebraic entanglement, and this explains why the regime $W \gg \Gamma_c$ has the maximal coherent information between the two degrees of freedom.

VI. CONCLUSION

In this paper, we explored the connection between algebraic entanglement and Lie group symmetries. We have shown

that one can exploit the structure of the irreps of compact Lie groups to perform operations in polynomial scaling that would typically require an exponentially-scaled complexity. In particular, we exploit the structure of a direct sum between irreps of $SU(2)$ to diagonalize density matrices in a block-by-block manner, the largest block scales as $O(N^2)$, and then exploit the multiplicity of the irreps to achieve a linear scaling of entropy with a Hilbert space whose dimensionality only has polynomial scaling. While we have focused on the case $SU(2) \otimes SU(2) < SU(4)$ here, our methodology can be readily generalized to $SU(m) \otimes SU(n) < SU(m \times n)$ systems, and thus $SU(\ell) \otimes SU(m) \otimes SU(n) \otimes \dots$ systems by tracing out subsystems one-by-one, with a suitable adaptation of the pyramid that explores all the irrep of the underlying degrees of freedom (e.g., utilizing Ref. [80]). This could directly relate to the exact calculation of algebraic entanglement entropy between different ensembles of superspins in partially permutational symmetric systems using the simulation technique of Ref. [95].

The most immediate application of our procedure is to quantum information science. Here, entanglement entropy is an indication that certain information processes can be performed, such as quantum teleportation [29] or device independent quantum key distribution for cryptography [96]. This can offer insight into the role and advantage of algebraic entanglement in quantum computing algorithms. Moreover, our procedure could help explore the role of quantum entanglement in well-known processes where entanglement is not usually thought of. For example, the role of spontaneous emission, i.e., entanglement with free-space electromagnetic modes, in laser cooling has recently been scrutinized [69–72], and generalizations of our procedure could shed insight into the entanglement between the subsystems (particles and cooling light field) and its relation to phase space compression of the particles. Lastly, there may be non-trivial connections between the rapid growth of algebraic entanglement entropy and information scrambling [97, 98]. There, information is non-locally dispersed across subsystems and has important implications for quantum chaos and black holes [99]. Therefore, efficient determination of algebraic entanglement entropy provides another avenue to understanding how entanglement and correlations are distributed in complex quantum many-body systems.

ACKNOWLEDGEMENTS

We would like to thank Simon B. Jäger, Peter Zoller, John Cooper, Gage W. Harmon, Haonan Liu, and Charles Marder for useful discussions. This material is based upon work supported by the U.S. Department of Energy, Office of Science, National Quantum Information Science Research Centers, Quantum Systems Accelerator (Award No. DE-SCL0000121), and by the National Science Foundation Grant Nos. 2016244 and 2317149.

Appendix A: The Single-Particle Operators

We consider the operators

$$\begin{aligned}\hat{\sigma}_j^{(+)} &= |1\rangle\langle 0|_j, & \hat{\sigma}_j^{(-)} &= |0\rangle\langle 1|_j, & \hat{\sigma}_j^x &= \hat{\sigma}_j^{(+)} + \hat{\sigma}_j^{(-)}, \\ \hat{\sigma}_j^y &= i\left(\hat{\sigma}_j^{(-)} - \hat{\sigma}_j^{(+)}\right), & \hat{\sigma}_j^z &= \left[\hat{\sigma}_j^{(+)}, \hat{\sigma}_j^{(-)}\right],\end{aligned}\quad (\text{A1})$$

on the J degree of freedom and

$$\begin{aligned}\hat{s}_j^{(+)} &= |\uparrow\rangle\langle \downarrow|_j, & \hat{s}_j^{(-)} &= |\downarrow\rangle\langle \uparrow|_j, & \hat{s}_j^x &= \hat{s}_j^{(+)} + \hat{s}_j^{(-)}, \\ \hat{s}_j^y &= i\left(\hat{s}_j^{(-)} - \hat{s}_j^{(+)}\right), & \hat{s}_j^z &= \left[\hat{s}_j^{(+)}, \hat{s}_j^{(-)}\right],\end{aligned}\quad (\text{A2})$$

on the K degree of freedom. Sums over these operators for each atom generates the operators in the respective $\mathfrak{su}(2)$ sub-algebras.

-
- [1] J. T. Reilly, J. D. Wilson, S. B. Jäger, C. Wilson, and M. J. Holland, Optimal generators for quantum sensing, *Phys. Rev. Lett.* **131**, 150802 (2023).
- [2] C. L. Degen, F. Reinhard, and P. Cappellaro, Quantum sensing, *Rev. Mod. Phys.* **89**, 035002 (2017).
- [3] M. Tse *et al.*, Quantum-enhanced advanced ligo detectors in the era of gravitational-wave astronomy, *Phys. Rev. Lett.* **123**, 231107 (2019).
- [4] E. Pedrozo-Peñafiel, S. Colombo, C. Shu, A. F. Adiyatullin, Z. Li, E. Mendez, B. Braverman, A. Kawasaki, D. Akamatsu, Y. Xiao, and V. Vuletić, Entanglement on an optical atomic-clock transition, *Nature* **588**, 414–418 (2020).
- [5] J. M. Robinson, M. Miklos, Y. M. Tso, C. J. Kennedy, T. Bothwell, D. Kedar, J. K. Thompson, and J. Ye, Direct comparison of two spin-squeezed optical clock ensembles at the 10^{-21} level, *Nature Physics* **20**, 208 (2024).
- [6] K. A. Gilmore, M. Affolter, R. J. Lewis-Swan, D. Barberena, E. Jordan, A. M. Rey, and J. J. Bollinger, Quantum-enhanced sensing of displacements and electric fields with two-dimensional trapped-ion crystals, *Science* **373**, 673 (2021).
- [7] J. T. Reilly, S. B. Jäger, J. D. Wilson, J. Cooper, S. Eggert, and M. J. Holland, Speeding up squeezing with a periodically driven dicke model, *Phys. Rev. Res.* **6**, 033090 (2024).
- [8] V. M. Kendon and W. J. Munro, Entanglement and its role in shor’s algorithm, *Quantum Info. Comput.* **6**, 630–640 (2006).
- [9] C. H. Bennett and S. J. Wiesner, Communication via one- and two-particle operators on einstein-podolsky-rosen states, *Phys. Rev. Lett.* **69**, 2881 (1992).
- [10] T. Schaetz, M. D. Barrett, D. Leibfried, J. Chiaverini, J. Britton, W. M. Itano, J. D. Jost, C. Langer, and D. J. Wineland, Quantum dense coding with atomic qubits, *Phys. Rev. Lett.* **93**, 040505 (2004).
- [11] J. Yin, Y.-H. Li, S.-K. Liao, M. Yang, Y. Cao, L. Zhang, J.-G. Ren, W.-Q. Cai, W.-Y. Liu, S.-L. Li, R. Shu, Y.-M. Huang, L. Deng, L. Li, Q. Zhang, N.-L. Liu, Y.-A. Chen, C.-Y. Lu, X.-B. Wang, F. Xu, J.-Y. Wang, C.-Z. Peng, A. K. Ekert, and J.-W. Pan, Entanglement-based secure quantum cryptography over 1,120 kilometres, *Nature* **582**, 501 (2020).
- [12] W.-Z. Liu, Y.-Z. Zhang, Y.-Z. Zhen, M.-H. Li, Y. Liu, J. Fan, F. Xu, Q. Zhang, and J.-W. Pan, Toward a photonic demonstration of device-independent quantum key distribution, *Phys. Rev. Lett.* **129**, 050502 (2022).
- [13] G. García-Pérez, M. A. C. Rossi, and S. Maniscalco, Ibm q experience as a versatile experimental testbed for simulating open quantum systems, *npj Quantum Information* **6**, 1 (2020).
- [14] C. Kokail, R. van Bijnen, A. Elben, B. Vermersch, and P. Zoller, Entanglement hamiltonian tomography in quantum simulation, *Nature Physics* **17**, 936 (2021).
- [15] B. Sundar, D. Barberena, A. P. n. Orioli, A. Chu, J. K. Thompson, A. M. Rey, and R. J. Lewis-Swan, Bosonic pair production and squeezing for optical phase measurements in long-lived dipoles coupled to a cavity, *Phys. Rev. Lett.* **130**, 113202 (2023).
- [16] M. K. Joshi, C. Kokail, R. van Bijnen, F. Kranzl, T. V. Zache, R. Blatt, C. F. Roos, and P. Zoller, Exploring large-scale entanglement in quantum simulation, *Nature* **624**, 539 (2023).
- [17] N. Euler and M. Gärttner, Detecting high-dimensional entanglement in cold-atom quantum simulators, *PRX Quantum* **4**, 040338 (2023).
- [18] R. Horodecki, P. Horodecki, M. Horodecki, and K. Horodecki, Quantum entanglement, *Rev. Mod. Phys.* **81**, 865 (2009).
- [19] E. M. Gauger, E. Rieper, J. J. L. Morton, S. C. Benjamin, and V. Vedral, Sustained quantum coherence and entanglement in the avian compass, *Phys. Rev. Lett.* **106**, 040503 (2011).
- [20] M. G. Genoni, S. Olivares, and M. G. A. Paris, Optical phase estimation in the presence of phase diffusion, *Phys. Rev. Lett.* **106**, 153603 (2011).
- [21] T. Ono, R. Okamoto, and S. Takeuchi, An entanglement-enhanced microscope, *Nature Communications* **4**, 2426 (2013).
- [22] N. Brunner, M. Huber, N. Linden, S. Popescu, R. Silva, and P. Skrzypczyk, Entanglement enhances cooling in microscopic quantum refrigerators, *Phys. Rev. E* **89**, 032115 (2014).
- [23] S. Apte, Quantum biology: Harnessing nano-technology’s last frontier with modified excipients and food ingredients, *Journal of Excipients and Food Chemicals* **5** (2016).
- [24] S. Ecker, F. Bouchard, L. Bulla, F. Brandt, O. Kohout, F. Steinhilber, R. Fickler, M. Malik, Y. Guryanova, R. Ursin, and M. Huber, Overcoming noise in entanglement distribution, *Phys. Rev. X* **9**, 041042 (2019).
- [25] A. Shankar, J. T. Reilly, S. B. Jäger, and M. J. Holland, Subradiant-to-subradiant phase transition in the bad cavity laser, *Phys. Rev. Lett.* **127**, 073603 (2021).
- [26] W.-Z. Liu, Y.-Z. Zhang, Y.-Z. Zhen, M.-H. Li, Y. Liu, J. Fan, F. Xu, Q. Zhang, and J.-W. Pan, Toward a photonic demonstration of device-independent quantum key distribution, *Phys. Rev. Lett.* **129**, 050502 (2022).
- [27] C. H. Bennett, G. Brassard, C. Crépeau, R. Jozsa, A. Peres, and W. K. Wootters, Teleporting an unknown quantum state via dual classical and einstein-podolsky-rosen channels, *Phys. Rev. Lett.* **70**, 1895 (1993).
- [28] W.-L. Li, C.-F. Li, and G.-C. Guo, Probabilistic teleportation and entanglement matching, *Phys. Rev. A* **61**, 034301 (2000).

- [29] X. Chen, Y. Shen, and F.-L. Zhang, Perfect teleportation with a partially entangled quantum channel, *Phys. Rev. A* **106**, 032430 (2022).
- [30] P. Hyllus, W. Laskowski, R. Krischek, C. Schwemmer, W. Wieczorek, H. Weinfurter, L. Pezzé, and A. Smerzi, Fisher information and multiparticle entanglement, *Phys. Rev. A* **85**, 022321 (2012).
- [31] J. Liu, H. Yuan, X.-M. Lu, and X. Wang, Quantum fisher information matrix and multiparameter estimation, *Journal of Physics A: Mathematical and Theoretical* **53**, 023001 (2019).
- [32] D. T. Smithey, M. Beck, M. G. Raymer, and A. Faridani, Measurement of the wigner distribution and the density matrix of a light mode using optical homodyne tomography: Application to squeezed states and the vacuum, *Phys. Rev. Lett.* **70**, 1244 (1993).
- [33] V. D’Auria, S. Fornaro, A. Porzio, S. Solimeno, S. Olivares, and M. G. A. Paris, Full characterization of gaussian bipartite entangled states by a single homodyne detector, *Phys. Rev. Lett.* **102**, 020502 (2009).
- [34] J. Bae, B. C. Hiesmayr, and D. McNulty, Linking entanglement detection and state tomography via quantum 2-designs, *New Journal of Physics* **21**, 013012 (2019).
- [35] A. Ekert and P. L. Knight, Entangled quantum systems and the schmidt decomposition, *American Journal of Physics* **63**, 415 (1995).
- [36] M. Nielsen and I. Chuang, *Quantum Computation and Quantum Information: 10th Anniversary Edition* (Cambridge University Press, 2010).
- [37] J. Eisert, M. Cramer, and M. B. Plenio, Colloquium: Area laws for the entanglement entropy, *Rev. Mod. Phys.* **82**, 277 (2010).
- [38] P. Calabrese and J. Cardy, Entanglement entropy and quantum field theory, *Journal of statistical mechanics: theory and experiment* **2004**, P06002 (2004).
- [39] A. Kitaev and J. Preskill, Topological entanglement entropy, *Phys. Rev. Lett.* **96**, 110404 (2006).
- [40] L. Masanes, All bipartite entangled states are useful for information processing, *Phys. Rev. Lett.* **96**, 150501 (2006).
- [41] R. F. Werner, Quantum states with einstein-podolsky-rosen correlations admitting a hidden-variable model, *Phys. Rev. A* **40**, 4277 (1989).
- [42] D. Girolami and G. Adesso, Observable measure of bipartite quantum correlations, *Phys. Rev. Lett.* **108**, 150403 (2012).
- [43] B. Coecke and A. Kissinger, The compositional structure of multipartite quantum entanglement, in *International Colloquium on Automata, Languages, and Programming* (Springer, 2010) pp. 297–308.
- [44] G. Tóth, Multipartite entanglement and high-precision metrology, *Phys. Rev. A* **85**, 022322 (2012).
- [45] Z. Ren, W. Li, A. Smerzi, and M. Gessner, Metrological detection of multipartite entanglement from young diagrams, *Phys. Rev. Lett.* **126**, 080502 (2021).
- [46] A. P. Balachandran, T. R. Govindarajan, A. R. de Queiroz, and A. F. Reyes-Lega, Algebraic approach to entanglement and entropy, *Phys. Rev. A* **88**, 022301 (2013).
- [47] A. F. Reyes-Lega, Entanglement entropy in quantum mechanics: An algebraic approach, in *Particles, Fields and Topology* (World Scientific Publishing Co., 2023) Chap. Chapter 18, pp. 191–199.
- [48] D. Pontello, Aspects of entanglement entropy in algebraic quantum field theory, arXiv preprint arXiv:2005.13975 (2020).
- [49] Y. Li, M. Gessner, W. Li, and A. Smerzi, Hyper- and hybrid nonlocality, *Phys. Rev. Lett.* **120**, 050404 (2018).
- [50] P. van Loock, W. J. Munro, K. Nemoto, T. P. Spiller, T. D. Ladd, S. L. Braunstein, and G. J. Milburn, Hybrid quantum computation in quantum optics, *Phys. Rev. A* **78**, 022303 (2008).
- [51] S. Takeda, M. Fuwa, P. van Loock, and A. Furusawa, Entanglement swapping between discrete and continuous variables, *Phys. Rev. Lett.* **114**, 100501 (2015).
- [52] U. L. Andersen, J. S. Neergaard-Nielsen, P. van Loock, and A. Furusawa, Hybrid discrete- and continuous-variable quantum information, *Nature Physics* **11**, 713 (2015).
- [53] A. E. Ulanov, D. Sychev, A. A. Pushkina, I. A. Fedorov, and A. I. Lvovsky, Quantum teleportation between discrete and continuous encodings of an optical qubit, *Phys. Rev. Lett.* **118**, 160501 (2017).
- [54] G. Guccione, T. Darras, H. L. Jeannic, V. B. Verma, S. W. Nam, A. Cavaillès, and J. Laurat, Connecting heterogeneous quantum networks by hybrid entanglement swapping, *Science Advances* **6**, eaba4508 (2020).
- [55] C. Shukla, P. Malpani, and K. Thapliyal, Hierarchical quantum network using hybrid entanglement, *Quantum Information Processing* **20**, 121 (2021).
- [56] F. Xu, M. Wang, C. Qiao, S. Li, H. Wang, and X. Su, Hybrid entanglement carrying orbital angular momentum, *Science Bulletin* **70**, 876 (2025).
- [57] J. D. Wilson, S. B. Jäger, J. T. Reilly, A. Shankar, M. L. Chiofalo, and M. J. Holland, Beyond one-axis twisting: Simultaneous spin-momentum squeezing, *Phys. Rev. A* **106**, 043711 (2022).
- [58] R. M. Gingrich and C. Adami, Quantum entanglement of moving bodies, *Phys. Rev. Lett.* **89**, 270402 (2002).
- [59] F. Jeske, T. Stöferle, and M. DeKieviet, Massive spin-momentum entanglement measured in an atomic beam spin echo experiment, *The European Physical Journal D* **63**, 25 (2011).
- [60] M. T. Manzoni, L. Mathey, and D. E. Chang, Designing exotic many-body states of atomic spin and motion in photonic crystals, *Nature Communications* **8**, 14696 (2017).
- [61] T. Stav, A. Faerman, E. Maguid, D. Oren, V. Kleiner, E. Hasman, and M. Segev, Quantum entanglement of the spin and orbital angular momentum of photons using metamaterials, *Science* **361**, 1101 (2018).
- [62] S. S. Kale, Y. Ding, Y. P. Chen, B. Friedrich, and S. Kais, Spin-momentum entanglement in a bose–einstein condensate, *Phys. Chem. Chem. Phys.* **22**, 25669 (2020).
- [63] G. P. Greve, C. Luo, B. Wu, and J. K. Thompson, Entanglement-enhanced matter-wave interferometry in a high-finesse cavity, *Nature* **610**, 472 (2022).
- [64] F. Finger, R. Rosa-Medina, N. Reiter, P. Christodoulou, T. Donner, and T. Esslinger, Spin- and momentum-correlated atom pairs mediated by photon exchange and seeded by vacuum fluctuations, *Phys. Rev. Lett.* **132**, 093402 (2024).
- [65] O. Chelpanova, K. Seetharam, R. Rosa-Medina, N. Reiter, F. Finger, T. Donner, and J. Marino, Dynamics of spin-momentum entanglement from superradiant phase transitions, *Phys. Rev. Res.* **6**, 033193 (2024).
- [66] F. Barkhausen, L. Ares, S. Schumacher, and J. Sperling, Entanglement between dependent degrees of freedom: Quasiparticle correlations, *Phys. Rev. A* **111**, 032404 (2025).
- [67] J. T. Reilly, G. W. Harmon, J. D. Wilson, M. J. Holland, and S. B. Jäger, Nonclassical many-body superradiant states with interparticle and spin-momentum entanglement (2026), (to be published).
- [68] A. M. Kaufman, M. E. Tai, A. Lukin, M. Rispoli, R. Schittko, P. M. Preiss, and M. Greiner, Quantum thermalization through entanglement in an isolated many-body system, *Science* **353**, 794 (2016).
- [69] H. Metcalf, Entropy exchange in laser cooling, *Phys. Rev. A* **77**, 061401 (2008).
- [70] C. Corder, B. Arnold, and H. Metcalf, Laser cooling without spontaneous emission, *Phys. Rev. Lett.* **114**, 043002 (2015).

- [71] J. P. Bartolotta, S. B. Jäger, J. T. Reilly, M. A. Norcia, J. K. Thompson, G. Smith, and M. J. Holland, Entropy transfer from a quantum particle to a classical coherent light field, *Phys. Rev. Res.* **4**, 013218 (2022).
- [72] J. T. Reilly, *Entropy Removal and Coherence with Lasers*, Bachelor's thesis, University of Colorado Boulder (2020).
- [73] M. Xu, D. A. Tieri, and M. J. Holland, Simulating open quantum systems by applying $\text{su}(4)$ to quantum master equations, *Phys. Rev. A* **87**, 062101 (2013).
- [74] A. Piñeiro Orioli, J. K. Thompson, and A. M. Rey, Emergent dark states from superradiant dynamics in multilevel atoms in a cavity, *Phys. Rev. X* **12**, 011054 (2022).
- [75] R. E. F. Silva and J. Feist, Permutational symmetry for identical multilevel systems: A second-quantized approach, *Phys. Rev. A* **105**, 043704 (2022).
- [76] D. A. Steck, *Quantum and atom optics* (2007).
- [77] X.-H. Li and S. Ghose, Self-assisted complete maximally hyperentangled state analysis via the cross-kerr nonlinearity, *Phys. Rev. A* **93**, 022302 (2016).
- [78] Z. Zeng, Complete analysis of the maximally hyperentangled state via the weak cross-kerr nonlinearity, *J. Opt. Soc. Am. B* **39**, 2272 (2022).
- [79] H. Georgi, *Lie Algebras In Particle Physics: from Isospin To Unified Theories*, *Frontiers in Physics* (Avalon Publishing, 1999).
- [80] M. Mathur, I. Raychowdhury, and R. Anishetty, $\text{Su}(n)$ irreducible schwinger bosons, *Journal of Mathematical Physics* **51**, 093504 (2010).
- [81] W. Pfeifer, *The Lie Algebras $\text{su}(N)$, An Introduction* (Birkhäuser, 2003).
- [82] G. Eichmann, *Lecture notes: Qcd and hadron physics* (2020).
- [83] In terms of Young tableaux, the irreps of both $\text{SU}(2)$ subgroups must have $(N/2 - J)$ many boxes in the second row indicating singlet pairs [79, 81, 82].
- [84] L. Mandel and E. Wolf, *Optical Coherence and Quantum Optics* (Cambridge University Press, 1995).
- [85] D. J. Griffiths, *Introduction to Quantum Mechanics*, 2nd ed. (Cambridge University Press, 2017).
- [86] A. Björck, Numerics of gram-schmidt orthogonalization, *Linear Algebra and its Applications* **197-198**, 297 (1994).
- [87] M. M. Wilde, *Quantum Information Theory* (Cambridge University Press, 2013).
- [88] N. J. Cerf and C. Adami, Negative entropy in quantum information theory, in *New Developments on Fundamental Problems in Quantum Physics*, edited by M. Ferrero and A. van der Merwe (Springer Netherlands, Dordrecht, 1997) pp. 77–84.
- [89] M. Horodecki, J. Oppenheim, and A. Winter, Quantum state merging and negative information, *Communications in Mathematical Physics* **269**, 107 (2007).
- [90] M. Kitagawa and M. Ueda, Squeezed spin states, *Phys. Rev. A* **47**, 5138 (1993).
- [91] B. Buča and T. Prosen, A note on symmetry reductions of the lindblad equation: transport in constrained open spin chains, *New Journal of Physics* **14**, 073007 (2012).
- [92] S. Lieu, R. Belyansky, J. T. Young, R. Lundgren, V. V. Albert, and A. V. Gorshkov, Symmetry breaking and error correction in open quantum systems, *Phys. Rev. Lett.* **125**, 240405 (2020).
- [93] M. Nairn, B. Olmos, and P. Solanki, Controlling emergent dynamical behavior via phase-engineered strong symmetries, arXiv preprint arXiv:2602.18563 (2026).
- [94] J. T. Reilly, S. B. Jäger, J. Cooper, and M. J. Holland, Fully collective superradiant lasing with vanishing sensitivity to cavity length vibrations, *Phys. Rev. Lett.* , (2026).
- [95] J. T. Lee, S. Cardenas-Lopez, S. J. Masson, R. Trivedi, and A. Asenjo-Garcia, Exact many-body quantum dynamics in one-dimensional baths via "superspins", arXiv preprint arXiv:2505.00588 (2025).
- [96] S. Pirandola, U. L. Andersen, L. Banchi, M. Berta, D. Bunandar, R. Colbeck, D. Englund, T. Gehring, C. Lupo, C. Ottaviani, J. L. Pereira, M. Razavi, J. S. Shaari, M. Tomamichel, V. C. Usenko, G. Vallone, P. Villoresi, and P. Wallden, *Advances in quantum cryptography*, *Adv. Opt. Photon.* **12**, 1012 (2020).
- [97] K. A. Landsman, C. Figgatt, T. Schuster, N. M. Linke, B. Yoshida, N. Y. Yao, and C. Monroe, Verified quantum information scrambling, *Nature* **567**, 61 (2019).
- [98] J.-H. Wang, T.-Q. Cai, X.-Y. Han, Y.-W. Ma, Z.-L. Wang, Z.-H. Bao, Y. Li, H.-Y. Wang, H.-Y. Zhang, L.-Y. Sun, Y.-K. Wu, Y.-P. Song, and L.-M. Duan, Information scrambling dynamics in a fully controllable quantum simulator, *Phys. Rev. Res.* **4**, 043141 (2022).
- [99] P. Hayden and J. Preskill, Black holes as mirrors: quantum information in random subsystems, *Journal of high energy physics* **2007**, 120 (2007).